



Ion Implantation in the Form of Layers: A Novel Method to Surface Properties

Muhammad Ahsan Shafique^{1*}, Z. Zaheer¹, S. Sharif², H. Taskeen², S. A. Shah², Athar Naeem Akhtar¹, G. Murtaza¹, Ghulam Farid^{3,4}

¹ Centre for Advanced Studies in Physics, Government College University Lahore, Pakistan

² Department of Physics, Forman Christian College University (FCCU), Lahore, Pakistan

³ Department of Applied Physics, University of Barcelona, C/Martí i Franquès, 1, 08028 Barcelona, Catalunya, Spain

⁴ ENPHOCAMAT Group, Institute of Nanoscience and Nanotechnology (IN2UB), University of Barcelona, C/Martí i Franquès, 1, 08028 Barcelona, Catalunya, Spain

ARTICLE INFO

Article History:

Received: July 25, 2022
Revised: August 29, 2022
Accepted: December 29, 2022
Available Online: December 31, 2022

Keywords:

Surface Modification
Hydrogen
Ion Implantation
Particle Accelerator
H Layers

ABSTRACT

In this study, a novel method was adopted to tailor the surface properties of iron. We attempted to increase the degradation rate of iron by H-induced damaging. Equal number of H ions were implanted in four samples using a 2MV Pelletron accelerator. But the ion distribution was varied in the iron matrix by adding H ion layers in successively increasing depths. Interesting outcomes, contrary to our assumption were observed. The open-circuit potential was observed to shift toward a stable side. The Tafel plot also revealed improved corrosion potential and decreased corrosion current by adding H layers. Crystallographic studies revealed improved crystallinity and a small shift in preferred orientation of crystal growth.

OPEN ACCESS

© 2022 The Authors, Published by iRASD. This is an Open Access article under the Creative Common Attribution Non-Commercial 4.0

*Corresponding Author's Email: muhammadahsan@gcu.edu.pk

1. Introduction

The importance of iron is well-known and it is being employed in various engineering applications due to superior mechanical properties, appropriate corrosion resistance at a wide range of pH, and availability at a cheaper cost (McNeill & Edwards, 2001; Nishikata, Ichihara, Hayashi, & Tsuru, 1997). Although the use of pure iron is limited due to stability issues because some applications demand extended stability and lesser density to strength ratio. Therefore, iron has been replaced by other materials like aluminum, magnesium, stainless steel and other alloys in various fields of applications. But this material is still being used in a large number of applications and the material scientists have always been working to counter its associated problems and to improve its properties for various applications.

The Hydrogen being smallest in the periodic table has a degree of freedom to diffuse into the lattice of almost every material even at a lower temperature (Alefeld, 1978). The diffused hydrogen tends to accumulate at some local position in host lattice and they cause micro-cracks by weakening the chemical bonds. The micro-cracks are formed due to the formation of gas bubbles, however, the nature of the produced gas bubbles depends upon the host material. The trapped bubble in host matrix exerts pressure on grain boundaries, pushing them away from each other (Song & Curtin, 2012; Xu & Zhang, 2017). This phenomenon leads to metal failure called hydrogen-induced embrittlement. HEDE (Hydrogen Enhanced de-cohesion) is another phenomenon which leads to crystal failure in a specific direction (cleavage). The failure is due to an accumulation of H atoms within certain regions of a crystal system, the accumulated H atoms tend to reduce cohesive forces of crystal lattice (Du et al., 2011). HELP (Hydrogen Enhanced Localized Plasticity) is a similar H

induced failure. In this case, the H atoms reduce the crystal resistance to dislocation motion (Myers et al., 1992). Several methods are being applied to make the metals susceptible to hydrogen embrittlement. The hydrogen embrittlement hinders the use of several metals in different applications (Han, Xue, Fu, & Zhang, 2019).

Corrosion is a similar phenomenon that eventually causes material failure. Unlike hydrogen embrittlement corrosion is a surface process. The surface atoms undergo unwanted chemical reactions with environmental species which leads to the formation of an oxide layer. The layer makes the surface passive to some extent. The corrosion phenomenon eventually causes material failure by weakening chemical bonds, loss of strength, and fatigue.

Electrochemical corrosion is another associated problem with iron which makes the iron lesser suitable for various applications. Iron is also an important biodegradable biomedical material because of biocompatibility, biocorrosibility and suitable mechanical properties (Hermawan, Alamdari, Mantovani, & Dubé, 2008; Li, Zheng, & Qin, 2014; Moravej & Mantovani, 2011). This material is also being studied for bio-resorbable orthopedic, cardiovascular implant and tissue engineering scaffold applications. The degradation rate of a biodegradable implant is important for clinical application. The material degradation rate should be synchronized to the healing process, and material should degrade after a specific time. Therefore, there should be some available techniques which could be employed to engineer the degradation rate of implant material.

Researchers are trying different techniques for the purpose. Huang et al (Huang, Zheng, & Han, 2016) observed enhanced the degradation rate of pure iron by zinc ion implantation. Abdul Hakeem et al proposed degradation rate can be tailored by incorporating biodegradable polymer into porous iron (Yusop, Daud, Nur, Kadir, & Hermawan, 2015). Wang et al also performed a similar study to enhance bio-corrosion, they found the incorporation of calcium silicate particles in the iron matrix to enhance the degradability (Wang et al., 2017). Waksman et al carried out an in-vivo study to investigate the compatibility of iron stents. They implanted bio-corrodible iron stents and cobalt-chromium stents randomly in coronary arteries of pigs. They found no adverse effects of bio-resorbable stents (Waksman, Pakala, Baffour, Seaborn, & Hellinga, 2008).

In our study, we attempted to accelerate the degradation rate of iron by the deteriorating effects of hydrogen. We implanted hydrogen ions into the lattice of pure iron in a novel way. We observed the results contrary to our assumption, the hydrogen implanted iron samples are found even more stable as compared to the samples with no hydrogen content. Interesting degradation behavior of pure iron is observed by changing the number of H layers in the iron matrix. Our study suggests the hydrogen layers formation with the appropriate number density of hydrogen atoms in the metallic matrix could reduce the degradation rate of hydrogen-induced cavities. Moreover, layers formation could be an effective technique to modify different surface properties.

2. Experimental Work

2.1. Sample Preparation

Five iron pieces having dimension 1.3cm×1cm and thickness 0.5 cm are cut from a sheet with the help of diamond wheel cutter. The samples are then grinded and polished using silicon carbide papers of different grits and diamond paste respectively. Finally, the samples are cleaned in ultrasonic bath in deionized water and then in acetone for 15 minute each.

2.2. H Ion Implantation

Ions are implanted at the same energy =300 keV in a single layer (ion density = 2×10^{14} ions/cm²). The same dose is given to the second sample but one half of the dose (ion density in the first layer = 1×10^{14} ions/cm²) is implanted at 300 keV and the other half (ion density in second layer = 1×10^{14} ions/cm²) is implanted at 350 keV which makes two ionic layers in the iron matrix. The number density of each layer becomes 1×10^{14} ions/cm². Similarly, in the third sample, the same dose is divided into three parts. Three layers are

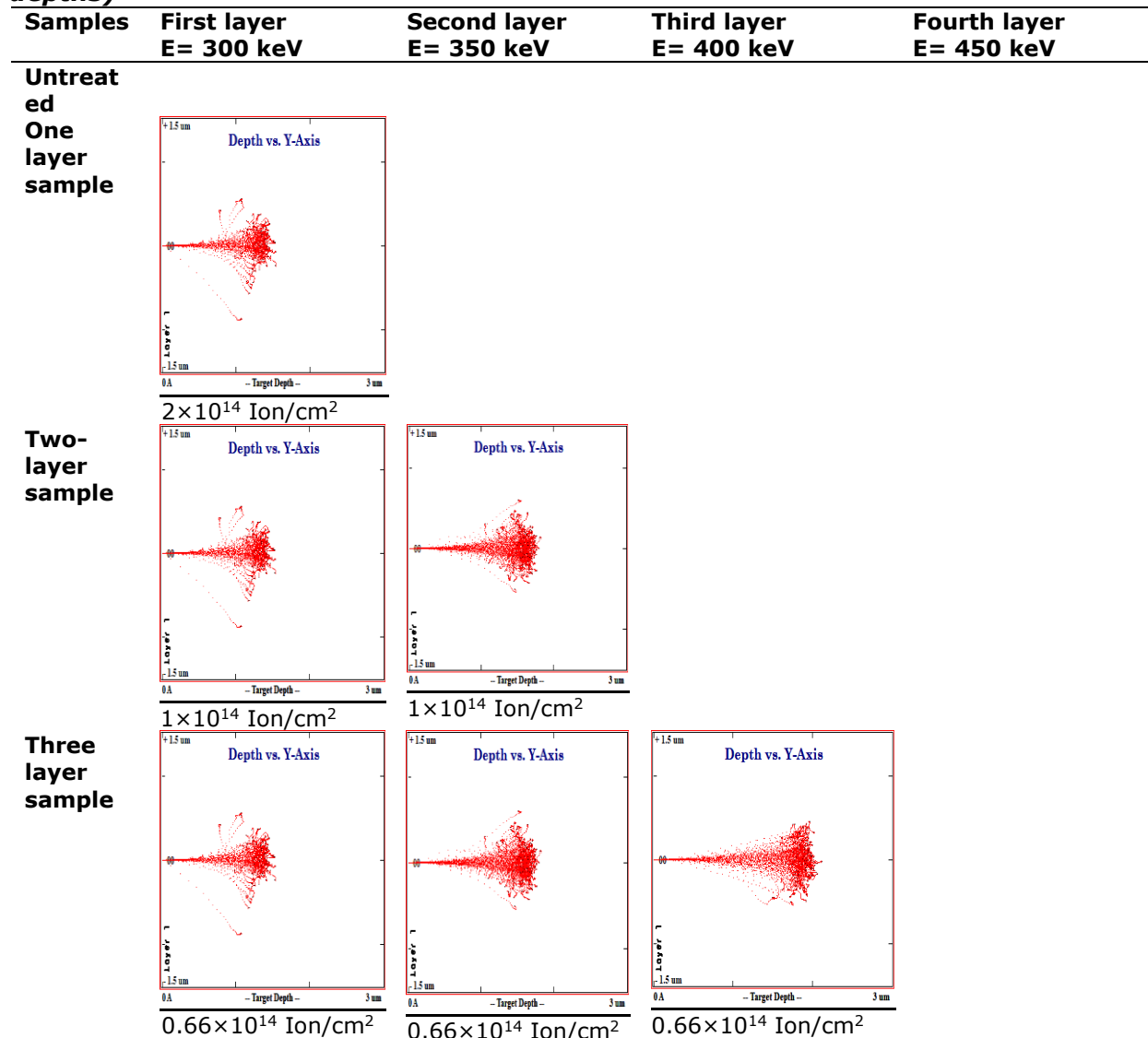
formed, the first ion layer is implanted at 300 keV, the second layer is implanted at 350 keV and the third layer at 400 keV (each layer contains 0.66×10^{14} Ion/cm²). Likewise, four layers are formed in the fourth sample, the detail of energy, range of ions and number density is mentioned in Table1”.

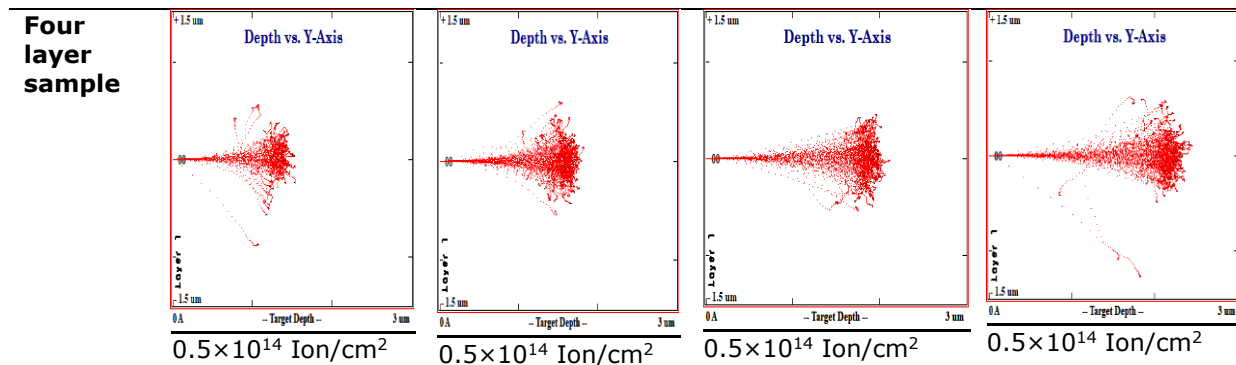
We believe that the layers formation in the material lattice by varying ion distribution keeping the sum constant is a new technique. In our experiment the number density of H ions per unit area of the target is decreased sequentially. By adding the energy steps different layers of H are formed in the iron matrix. The ion ranges are estimated using SRIM simulation (Ziegler, Ziegler, & Biersack, 2010). The different range profiles at different energies are given in table1 (a).

Table 1
Ion distribution in different layers and projected ranges of ions at different energy steps (SRIM calculations)

Samples	Number of ion Implanted (Ion/cm ²)	Energy steps (keV)	Projected Range(μm)
Untreated	0	0	0
One layer sample	2×10^{14}	300	1.32
Two layer sample	$(1 + 1) \times 10^{14} = 2 \times 10^{14}$	300+350	1.32+1.58
Three layer sample	$(0.66 + 0.66 + 0.66) \times 10^{14} = 2 \times 10^{14}$	300+350+400	1.32+1.58+1.85
Four layer sample	$(0.5 + 0.5 + 0.5 + 0.5) \times 10^{14} = 2 \times 10^{14}$	300+350+400 +450	1.32+1.58+1.85 +2.14

Table1 (a)
SRIM simulation profiles at different energies (H ion concentrations in different depths)





2.3. Ion Dose Calculation

$$\text{Dose/sec} = (\text{beam current} \times \text{Number of charges in 1 coulomb}) \div \text{beam size}$$

$$\text{Dose} = [(I \times 6.3 \times 10^{18}) \div \text{beam size}] \times \text{time of exposure}$$

3. Characterization Techniques

"The XRD analysis is carried out using PANalytic Xpert pro diffractometer. Cu K α (1.541Å) radiations are used at 40KV and 30mA for structural analysis. The diffraction profiles are recorded in glancing incident mode in 2 θ range from 20 $^\circ$ to 80 $^\circ$ with a step size of 0.02 $^\circ$ and total 3000 points are taken for each sample. Gamry potentiostat (1000E) is used for electrochemical studies of samples. The potentiostat contains a three-electrode cell setup, the prepared samples are used as working electrodes. Ag/AgCl is used as reference electrode and graphite is used as counter electrode. All the electrochemical measurements are carried out at 35 $^\circ$ C in Ringer lactate solution. Scanning electron microscope (SEM) JEOL JSM 6480LV is used in SEI mode (Accelerating voltage=20KV) for topographic studies of samples".

4. Results and Discussion

4.1. XRD Studies

The XRD analysis is performed to investigate the impact of ion implantation on various crystallographic parameters by H ion implantation. The X-Ray probe depth is estimated using the software *XPert high score plus* with MAC calculator. The penetration depth is found 5.1 μ m.

The XRD profiles are shown in Fig1. The signature diffraction peaks of Fe [110] and [200] are observed at 2 θ position approximately equal to 44.56 $^\circ$ and 65.404 $^\circ$ respectively. The profile suggests that the preferred orientation of growth is [110] direction. The addition of the number of H layers increases the intensity of [110] peak while the intensity of [200] plane decreases. The maximum intensity of [200] plane is observed in as received sample (\approx 18.65%) while the minimum [200] peak intensity is observed in the sample implanted with 4 H ion layers (\approx 4.0%). This suggests that H ions in Fe lattice encourage rearrangement of crystal lattice. This is also visible in the texture coefficient profile Fig2. The alteration in the preferred orientation of growth is due to the energy distribution in the crystal lattice. The energy of incoming H ions dissipates in the lattice, allowing the grains to rearrange. During the rearrangement process, the grains tend to settle at the minimum energy position by changing the angle with respect to the previous position. A similar reason for the rearrangement of crystal planes is the decreased crystallite size. The surface of the grain boundary possesses some free energy due to unsatisfied bonds at the boundary. A greater number of grains per unit volume results in a larger number of grain boundaries. Therefore, to attain equilibrium position the grains tend to rearrange. The peak broadening is not observed in XRD profiles. This indicates that the H ion does not trigger randomness or amorphization in iron lattice. The deeper penetration of H ions requires greater energy to overcome the Coulomb barrier of electronic cloud and nuclear potential.

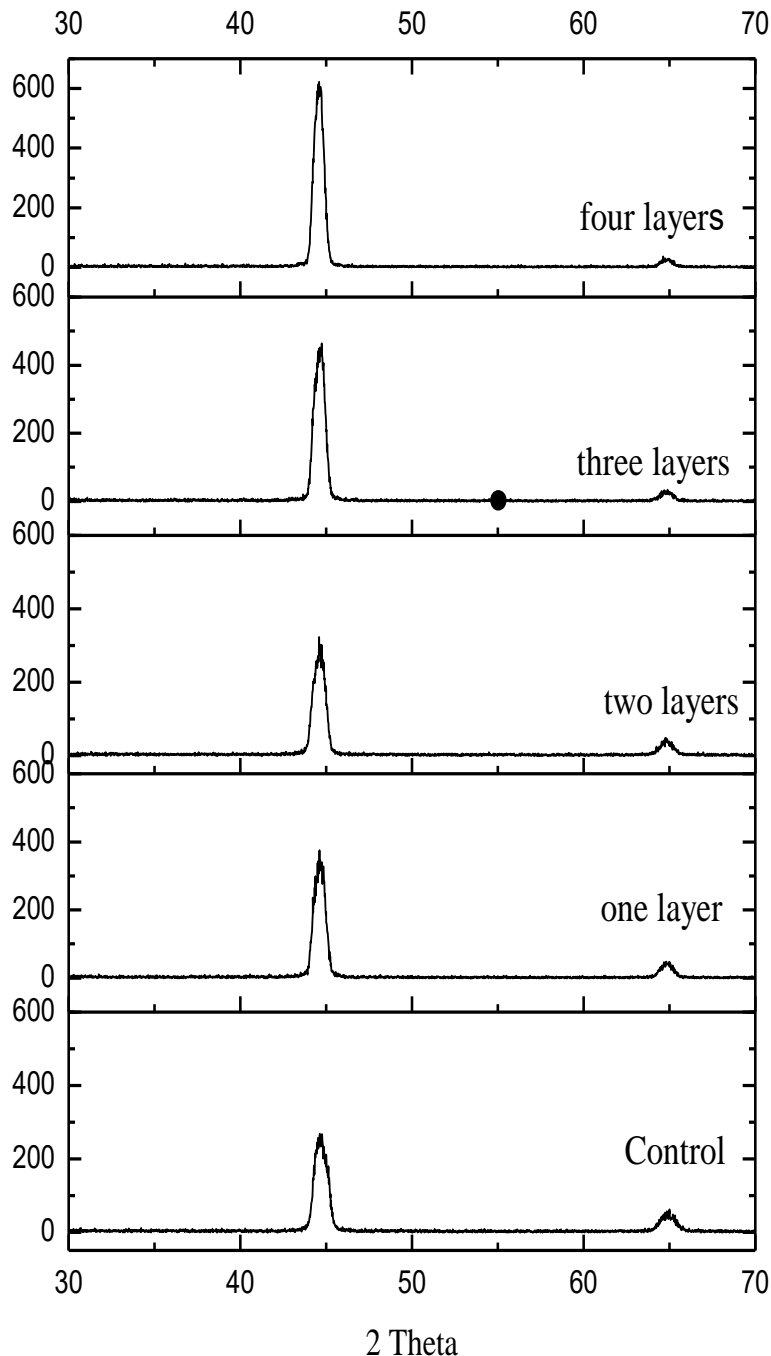


Figure 1: XRD profiles of samples treated with different H layers

The energy of incoming H ion dissipates in target lattice by multiple factors; in primary collisions with target nuclei, to overcome the electrostatic potential of electrons and protons. The primary collision mobilizes the target nuclei which perform further collisions with neighboring nuclei called secondary collision. The phenomenon results in a quasi-unstable local region which is at a higher energy state. The energy in the region allows the lattice to relax and rearrange. Akshaya et al (Behera, Facsko, Bandyopadhyay, Das, & Chatterjee, 2014) working in lower energy (50 keV) regime found amorphization by nitrogen ion implantation at lower fluence (10^{15} ions/cm²) and remarkable crystallization at higher fluence (10^{16} ions/cm²). Rafique et al (Rafique, Butt, & Ahmad, 2017) reported greater peak intensity by H ion implantation in Zircaloy-4. Naguib et al working in lower energy range 2-35 keV (Naguib & Kelly, 1970) found crystallization in amorphous ZrO₂ substrates by Kr implantation. Makinson et al (J D. Makinson, 2000) studied the diffraction patterns from the defects containing crystals by a computational technique. They concluded that the presence of point defects in crystal lattice decreases the peak intensity.

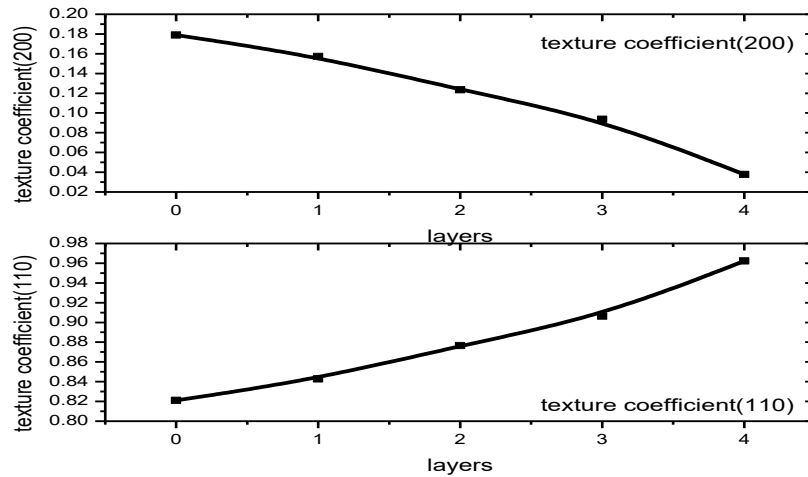


Figure 2: Variation in texture coefficient of (110) and (200) planes versus no of H layers

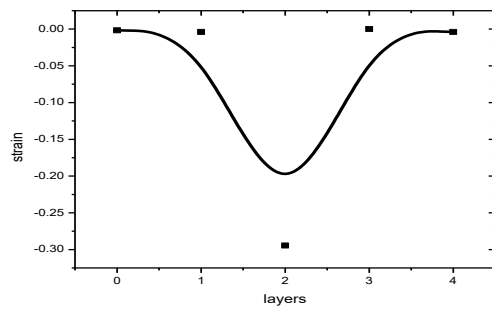


Figure 3(a): Variation in strain versus H layers

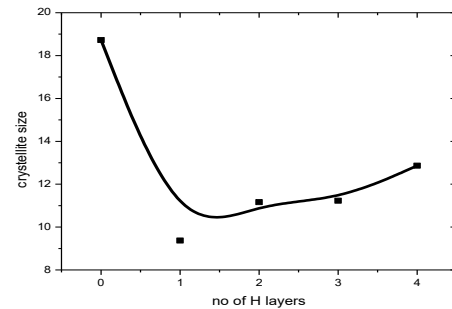


Figure 3(b): Variation in crystallite size versus H layers

Lesser energy of incoming ions allows the energy distribution and localized annealing in a smaller region. Increasing ion energy in different steps allows the energy distribution in a greater region of the target material. The crystallite size as a function of H ion penetration depth is mentioned in Fig3 (b). The profile suggests that the crystallite size decreases by increasing the depth of implanted H ions. The smaller crystallite size is representative of the presence of imperfection in the lattice. The size of H ions is very small as compared to the volume of the unit cell or the size of atoms in host lattice, therefore, it does not change the volume of cell or cell distortion consequently imparting no strain as shown in Fig3(a). There is no peak shifting as well which reveal H implantation has mild effects on the shape and size of the unit cell. The decreased crystallite size is attributed to the impact of accumulated H ions at grain boundaries.

4.2. Electrochemical Study

4.2.1. Initial Open Circuit Potential (OCP)

The electrochemical studies are performed to predict the stability of fabricated samples in the Ringer lactate solution. OCP profiles of treated and controlled samples is given in Fig4. OCP value determines the initial stability of the samples; greater the OCP value stable will be the material. The OCP value of untreated samples lies in the middle of the figure. The OCP value shifts toward negative side by adding the entire H ion dose in a single layer. This is least stable sample it has a minimum OCP value ($\approx -0.40V$). The initial OCP dramatically increases (shift to a lesser negative value) by adding a second layer of H^+ in the iron lattice, in this case, the ion dose is same but divided into two regions by adding an energy step.

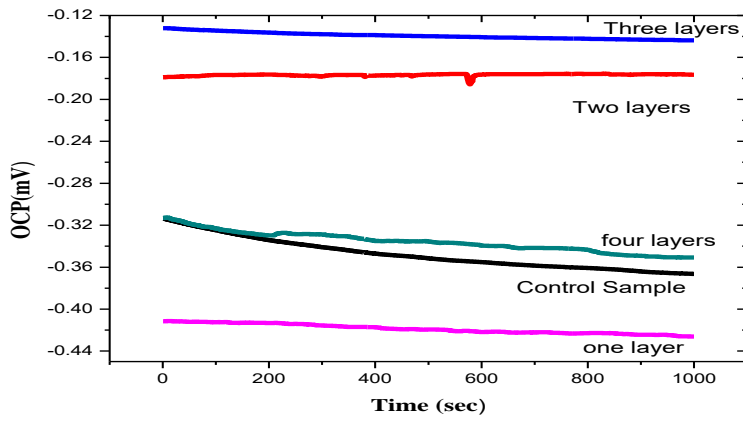


Figure 4: Variation in open circuit potential of different samples with time

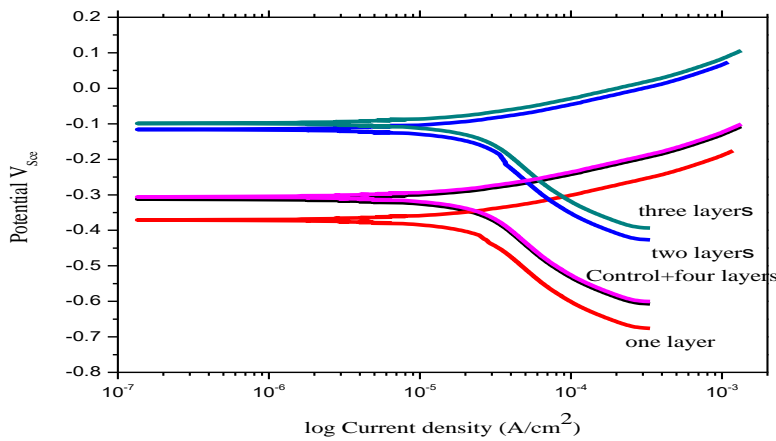


Figure 5: Tafel plots of treated and untreated samples

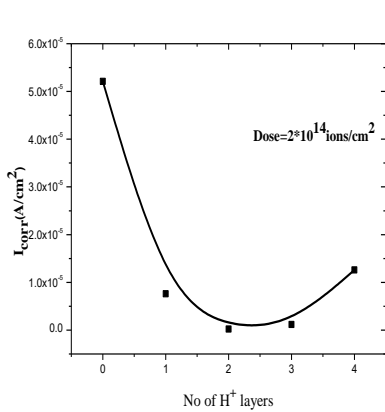


Figure 5(a): Variation in corrosion current with number of H layers

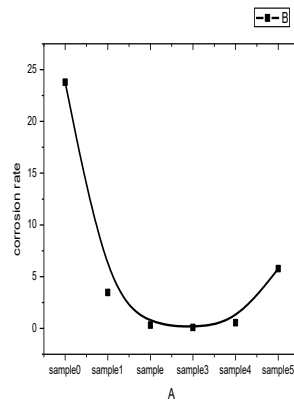


Figure 5(b): Variation in corrosion rate with number of H layers

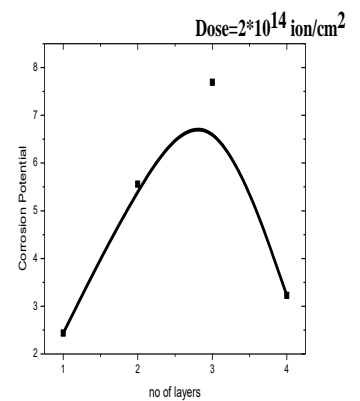


Figure 5(c): variation in corrosion potential with H layers

Further addition of a third layer further increases the OCP value. This is the threshold after this addition of another layer cause, a dramatic decrease of initial OCP value to the middle of the profiles, approximately equal to the value of untreated samples ($\approx -300\text{mV}$). The graph of treated samples representing OCP versus no of layers at the same dose is shown in Fig4. The sample implanted with three H^+ layers is found to be the most stable sample, while the sample with one H^+ is found most unstable samples (Zhu et al., 2009). The improved stability is due to the formation of protective H layers in iron lattice. The prepared ion layers hinder lattice distortion by stopping atomic diffusion across the layer. Xu et al restricted the hydrogen diffusion in the iron lattice by trapping hydrogen atoms in the vacancies produced by irradiation. They consequently observed suppressed hydrogen embrittlement (Xu & Zhang, 2017).

In our study, the abrupt decrease in OCP is attributed to the high energy of incoming H ions (the fourth energy step 450 keV). For the four layers sample, the energy carried by incoming H ions for the formation of fourth layers is highest among all the other ion energies (450 keV). While dissipating this larger amount of energy the incoming ions perform a greater number of the primary collision before coming to rest. The greater primary collision yields more displaced atoms in the lattice, which perform more secondary collisions. A bigger collision cascade is formed. Consequently, the bigger collision cascade disturbs other layers formed by lower energy H ions.

4.2.2. Potentiodynamic Polarization

Potentiodynamic polarization (PP) study is carried out to investigate corrosion kinetics parameters of controlled and treated samples. The Potentiodynamic polarization profiles are shown in Fig5. The corrosion parameters are calculated from PP profiles by Tafel extrapolation, different parameters are listed in Table2. Corrosion current (I_{corr}) is plotted against the number of layers in Fig. I_{corr} profile clearly indicates a decrease in corrosion rate by increasing the number of H layers without changing the ion dose. Maximum corrosion current (I_{corr}) is observed in the controlled sample suggesting the most unstable sample. The samples having two and three proton layers are the most stable samples among all the samples under study. Then the trend changes as the sample with four layers come up with a higher value of $I_{corr} \approx 12.60 \times 10^{-6} \text{ A/cm}^2$. A similar profile is observed by plotting corrosion rate against proton layers in Fig5 (b), which signifies layers formation by increasing ion energy induces surface stability. The surface stability increases up to energy limit of 400 keV, however, the surface stability decreases for 450 keV energy step, as the corrosion rate shift from 0.536 mpy to 5.762 mpy. The corrosion potential, corrosion current and corrosion rate studies are consistent with each other.

Implanted hydrogen ion gets trapped in the iron lattice at vacancy and/or interstitial position, which may lead to the formation of Fe-H complexes. Lv et al reported by a theoretical simulation that the hydrogen atoms are very stable in the iron lattice at the vacancy position (Lv, Zhang, Zhang, & Su, 2018). The locked hydrogen changes some mechanical properties of host lattice; it is reported the incorporation of H atom in iron produces stress, strain, brittleness, and hardness (Hiroshi Nakazawa, 2011). In single layer deposition, Fe-H complexes are distributed within the smaller volume of the iron matrix, therefore the number density is greater in comparison to multiple layer samples. The greater number density tends to deteriorate and destabilize the crystal structure. Evenly distributed Fe-H complexes in larger volume lead to the formation of a stable ordered structure as seen in XRD patterns. Another reason for enhanced stability may be the incorporation of H atoms at vacancy and/ or interstitial sites produces a protective layer. The protective layer hinders the further diffusion of H atoms as reported by Xu (Xu & Zhang, 2017). In our study, multiple H layers yield multiple protective shields consequently enhanced stability.

4.3. SEM Studies

SEM studies are performed after electrochemical corrosion study of control and treated samples. The analysis is performed to investigate the surface morphologies after corrosion studies. The SEM micrographs of untreated and treated samples are shown in Fig6. The corrosion products and pits are visible on all the treated and untreated samples. The corrosion products form different morphologies on different samples. A sponge-like morphology is observed in the untreated sample which is due to the rapid removal of gases from the surface as a result of corrosion. This signifies a higher corrosion rate in the untreated sample. The typical sponge shape morphology is not observed in any treated sample but the craters and dimples of different shapes and densities are observed which indicated pitting corrosion. Typical shapes of the linear cracks are not seen in any micrograph which indicates there is no hydrogen-induced damage or hydrogen embrittlement.

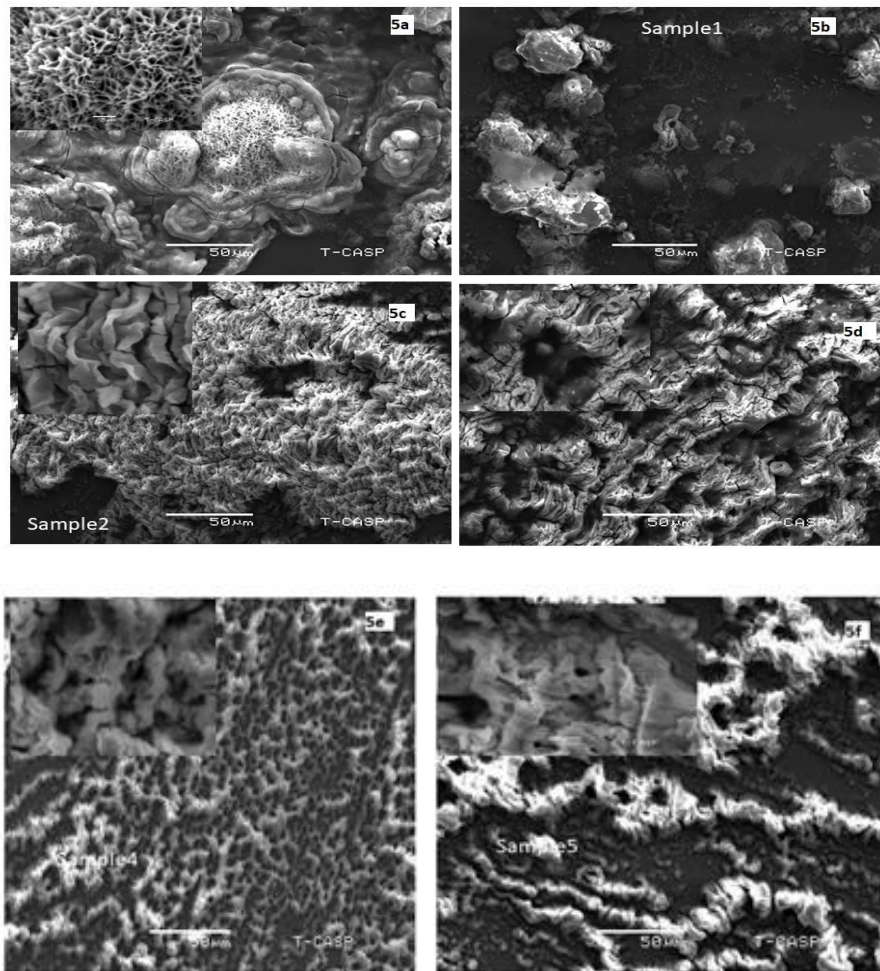


Figure 6: SEM micrograph of untreated and treated samples: Fig 5a: Untreated sample revealing sponge-like structures due to removal of gases during the corrosion process. Fig 5b,5c, 5d,5e and 5f showing pores and corrosion products. The cracks are not observed in any micrograph

Conclusion

H ions are made to reside within different depths of the iron matrix by giving them different energies. This form different proton-rich region. In the first sample, all the protons are implanted in a single region called a single layer, while in the second sample, the same ion dose is distributed in two different depths forming two proton layers. Similarly, an equal sum of H ions is distributed in three and four layers. The varied number density of implanted H ions changes the orientation of crystal growth. The decreased crystallite size is attributed to the impact of accumulated H ions at grain boundaries. The improved corrosion potential and decreased corrosion current by adding H layers is observed using Tafel plot. The electrochemical studies reveal decreased corrosion current, corrosion rate, and enhanced corrosion potential by changing the number of H ion layers, the study suggests the H layers serve as a protective shield to hinder material degradation.

Acknowledgment

The authors are thankful to ORIC, GC University Lahore for providing funding and Centre for advanced studies in physics (CASP) for providing access to particle accelerator and SEM facility.

References

- Alefeld, J. V. a. G. (1078). Diffusion of Hydrogen in Metals* *Applied Physics*, 28.
 Behera, A. K., Facsko, S., Bandyopadhyay, M. K., Das, S., & Chatterjee, S. (2014).
 Amorphization and recrystallization of single-crystalline hydrogen titanate nanowires

- by N⁺ ion irradiation. *Journal of Applied Physics*, 115(23), 233505. doi:10.1063/1.4884677
- Du, Y. A., Ismer, L., Rogal, J., Hickel, T., Neugebauer, J., & Drautz, R. (2011). First-principles study on the interaction of H interstitials with grain boundaries in α - and γ -Fe. *Physical Review B*, 84(14), 144121. doi:10.1103/PhysRevB.84.144121
- Han, Y., Xue, S., Fu, R., & Zhang, P. (2019). Effect of hydrogen content in ER5183 welding wire on the tensile strength and fracture morphology of Al–Mg MIG weld. *Vacuum*, 166, 218-225. doi:<https://doi.org/10.1016/j.vacuum.2019.05.011>
- Hermawan, H., Alamdari, H., Mantovani, D., & Dubé, D. (2008). Iron–manganese: new class of metallic degradable biomaterials prepared by powder metallurgy. *Powder Metallurgy*, 51(1), 38-45. doi:10.1179/174329008X284868
- Hiroshi Nakazawa, M. I. (2011). Fe–H Complexes in Catalysis. *Topics in Organometallic Chemistry*, 33, 27-81.
- Huang, T., Zheng, Y., & Han, Y. (2016). *Accelerating degradation rate of pure iron by zinc ion implantation* (Vol. 3).
- J D. Makinson, J. S. L., S.H. Magner, R.J. De Angelis. (2000). X-Ray Diffraction Signatures of Defects in Nanocrystalline Materials *Advances in X-ray Analysis*, 42.
- Li, H., Zheng, Y., & Qin, L. (2014). Progress of biodegradable metals. *Progress in Natural Science: Materials International*, 24(5), 414-422. doi:<https://doi.org/10.1016/j.pnsc.2014.08.014>
- Lv, G., Zhang, M., Zhang, H., & Su, Y. (2018). Hydrogen diffusion and vacancy clusterization in iron. *International Journal of Hydrogen Energy*, 43(32), 15378-15385. doi:<https://doi.org/10.1016/j.ijhydene.2018.06.075>
- McNeill, L. S., & Edwards, M. (2001). IRON PIPE CORROSION IN DISTRIBUTION SYSTEMS. *Journal - American Water Works Association*, 93(7), 88-100. doi:10.1002/j.1551-8833.2001.tb09246.x
- Moravej, M., & Mantovani, D. (2011). Biodegradable Metals for Cardiovascular Stent Application: Interests and New Opportunities. *International Journal of Molecular Sciences*, 12(7), 4250-4270. doi:10.3390/ijms12074250
- Myers, S. M., Baskes, M. I., Birnbaum, H. K., Corbett, J. W., DeLeo, G. G., Estreicher, S. K., . . . Stavola, M. J. (1992). Hydrogen interactions with defects in crystalline solids. *Reviews of Modern Physics*, 64(2), 559-617. doi:10.1103/RevModPhys.64.559
- Naguib, H. M., & Kelly, R. (1970). The crystallization of amorphous ZrO₂ by thermal heating and by ion bombardment. *Journal of Nuclear Materials*, 35(3), 293-305. doi:[https://doi.org/10.1016/0022-3115\(70\)90213-8](https://doi.org/10.1016/0022-3115(70)90213-8)
- Nishikata, A., Ichihara, Y., Hayashi, Y., & Tsuru, T. (1997). Influence of Electrolyte Layer Thickness and pH on the Initial Stage of the Atmospheric Corrosion of Iron. *Journal of The Electrochemical Society*, 144(4), 1244-1252. doi:10.1149/1.1837578
- Rafique, M., Butt, M. Z., & Ahmad, S. (2017). Investigation of morphological, structural, and mechanical characteristics of Zircaloy-4 irradiated with 3.5 MeV hydrogen ions beam. *Materials Research Express*, 4(9), 096507. doi:10.1088/2053-1591/aa8ae9
- Song, J., & Curtin, W. A. (2012). Atomic mechanism and prediction of hydrogen embrittlement in iron. *Nature Materials*, 12, 145. doi:10.1038/nmat3479
<https://www.nature.com/articles/nmat3479#supplementary-information>
- Waksman, R., Pakala, R., Baffour, R., Seaborn, R., & Hellinga, D. (2008). Short-Term Effects of Biocorrosible Iron Stents in Porcine Coronary Arteries. *Journal of Interventional Cardiology*, 21(1), 15-20. doi:10.1111/j.1540-8183.2007.00319.x
- Wang, S., Xu, Y., Zhou, J., Li, H., Chang, J., & Huan, Z. (2017). In vitro degradation and surface bioactivity of iron-matrix composites containing silicate-based bioceramic. *Bioactive Materials*, 2(1), 10-18. doi:<https://doi.org/10.1016/j.bioactmat.2016.12.001>
- Xu, Q., & Zhang, J. (2017). Novel Methods for Prevention of Hydrogen Embrittlement in Iron. *Scientific Reports*, 7(1), 16927. doi:10.1038/s41598-017-17263-8
- Yusop, A. H. M., Daud, N. M., Nur, H., Kadir, M. R. A., & Hermawan, H. (2015). Controlling the degradation kinetics of porous iron by poly(lactic-co-glycolic acid) infiltration for use as temporary medical implants. *Scientific Reports*, 5, 11194. doi:10.1038/srep11194
- Zhu, S., Huang, N., Xu, L., Zhang, Y., Liu, H., Sun, H., & Leng, Y. (2009). Biocompatibility of pure iron: In vitro assessment of degradation kinetics and cytotoxicity on

endothelial cells. *Materials Science and Engineering: C*, 29(5), 1589-1592.

doi:<https://doi.org/10.1016/j.msec.2008.12.019>

Ziegler, J. F., Ziegler, M. D., & Biersack, J. P. (2010). SRIM – The stopping and range of ions in matter (2010). *Nuclear Instruments and Methods in Physics Research Section B: Beam Interactions with Materials and Atoms*, 268(11), 1818-1823.

doi:<https://doi.org/10.1016/j.nimb.2010.02.091>